

Site-matched assessment of structural and tissue properties of cortical bone using scanning acoustic microscopy and synchrotron radiation μ CT

K Raum^{1,2}, I Leguerney¹, F Chandelier¹, M Talmant¹, A Saïed¹,
F Peyrin^{3,4} and P Laugier¹

¹ Laboratoire d'Imagerie Paramétrique, CNRS/Université Paris 6, UMR 7623, 15, rue de l'École de Médecine, 75006 Paris, France

² Q-BAM Group, Department of Orthopedics, Martin Luther University of Halle-Wittenberg, Magdeburger Straße 22, 06097 Halle, Germany

³ CREATIS; CNRS, UMR 5515; INSERM, U630; INSA, 69621 Villeurbanne Cedex, France

⁴ ESRF, BP 220, 38043 Grenoble Cedex, France

E-mail: kay.raum@medizin.uni-halle.de

Received 23 June 2005, in final form 18 October 2005

Published 19 January 2006

Online at stacks.iop.org/PMB/51/733

Abstract

200 MHz scanning acoustic microscopy (SAM) and synchrotron radiation μ CT (SR- μ CT) were used to assess microstructural parameters and tissue properties in site-matched regions of interest in cortical bone. Anterior and postero-lateral regions of ten cross sections from human cortical radius were explored. Structural parameters, including diameter and number of Haversian canals per cortical area (Ca.Dm, N.Ca/Ar) and porosity Po were assessed with both methods using a custom-developed image fusion and analysis software. Acoustic impedance Z and degree of mineralization of bone DMB were extracted separately for osteonal and interstitial tissues from the fused images. Structural parameter estimations obtained from radiographic and acoustic images were almost identical. DMB and impedance values were in the range between 0.77 and 1.28 g cm⁻³ and 5.13 and 12.1 Mrayl, respectively. Interindividual and regional variations were observed, whereas the strongest difference was found between osteonal and interstitial tissues (Z : 7.2 ± 1.1 Mrayl versus 9.3 ± 1.0 Mrayl, DMB: 1.06 ± 0.07 g cm⁻³ versus 1.16 ± 0.05 g cm⁻³, paired t -test, $p < 0.05$). Weak, but significant correlations between DMB and Z were obtained for the osteonal ($R^2 = 0.174$, $p < 10^{-4}$) and for the pooled (osteonal and interstitial) data. The regression of the pooled osteonal and interstitial tissue data follows a second-order polynomial ($R^2 = 0.39$, $p < 10^{-4}$). Both modalities fulfil the requirement for a simultaneous evaluation of cortical bone microstructure and material properties at the tissue level. While SAM inspection is limited to the evaluation of carefully prepared sample surfaces, SR- μ CT provides volumetric information on the tissue without substantial

preparation requirements. However, SAM provides a quantitative estimate of elastic properties at the tissue level that cannot be captured by SR- μ CT.

1. Introduction

It is now well accepted that not only bone quantity but also bone quality needs to be characterized to elucidate sparsely understood mechanisms involved in bone alteration due to several conditions such as physical condition, nutrition, age, genetic background, pathologies and treatment.

Bone quality, a poorly defined property, depends on a multiplicity of factors. Microstructure, mineralization, microdamage, composition and structure of the organic and mineral phases as well as their mutual interaction contribute to bone quality. The need for novel inspection techniques to investigate the different aspects of bone quality at a microstructural or ultrastructural level has emerged. High-resolution imaging modalities, e.g. micro-computed tomography (μ CT: Wachter *et al* 2001, 2002), synchrotron radiation μ CT (SR- μ CT: Hengsberger *et al* 2003, Bousson *et al* 2004, Peyrin *et al* 2001) and micro-magnetic resonance imaging (μ MRI: Pothuau *et al* 2002), have been applied in addition to histomorphometric analysis for assessing three-dimensional (3D) microstructural properties *in vitro*. Among them, x-ray microradiography (Boivin and Meunier 2002) and monochromatic SR- μ CT (Peyrin *et al* 2001) measurements provide complementary information about mineralization at the tissue level in 2D or 3D, respectively.

However, the main limitation of these techniques is their inability to quantitatively image bone elastic properties at the tissue level. Nanoindentation (Xu *et al* 2003, Zysset *et al* 1999) and acoustic microscopy (Raum *et al* 2004) are directed at measuring material elastic properties and its anisotropy. Whereas scanning acoustic microscopy can provide an image of acoustic impedance, a parameter related to tissue elasticity (Hofmann *et al* 2006), of a 2D surface, nanoindentation provides estimates of Young's modulus at a limited number of points only.

The choice of ultrasonic techniques to evaluate bone mechanical properties offers advantages over direct biomechanical testing given its nondestructive character (avoiding damage to the material during the test). Multi-scale evaluation can also be performed spanning a wide range of ultrasonic frequencies. The spatial resolution of high-frequency scanning acoustic microscopes (SAM) competes with that of other micro-imaging modalities. The acoustic impedance Z derived from the confocal reflection amplitude can be measured in two dimensions with a resolution comparable to the acoustic wavelength, e.g. 25 μ m at 50 MHz (Raum *et al* 2004) and better than 2 μ m at 900 MHz (Raum *et al* 2003). Therefore, acoustic microscopy may be suited to explore not only bone microstructure, but also material properties at a tissue level.

The current study was undertaken to validate acoustic microscopic assessment of cortical bone microstructure using reference data obtained on the same set of bone specimen with SR- μ CT. It will be followed by a second study dedicated to the extraction of tissue elasticity from acoustic measurements. Here, acoustic impedance distributions of human cortical bone samples obtained at 200 MHz were spatially mapped at a pixel size of 4 μ m and compared with site-matched mineral density maps obtained from 3D SR- μ CT data at a voxel size of 4.9 μ m. Structural parameters, e.g. diameter and number of Haversian canals per cortical area (Dm.Ca, N.Ca/Ar) and porosity Po , were assessed and compared with both methods.

The relation between acoustic impedance Z and degree of mineralization of bone DMB was investigated separately for osteonal and interstitial cortical tissues.

2. Materials and methods

2.1. Samples

The sample population included 2 female and 8 male radii from human cadaver donors of age between 68 and 90 years (75.9 ± 6.8 years). From each radius, a cross section was cut from the distal part of the diaphysis. The sections were then fixed with Technovit[®] 3040 resin (Heraeus Kulzer, Hanau, Germany) on special sample holders. After shock freezing sample and holder in liquid nitrogen, flat tissue surfaces were prepared for ultrasonic inspection using an ultra milling machine (Reichert Jung Ultrafräse, Leica GmbH, Bensheim, Germany). After several cycles of freezing and thawing cracks in the surrounding resin, but not in bone tissue, were observed. Other groups have shown that freezing does not alter the elastic properties of bone tissue (Linde and Sorensen 1993, Pelker *et al* 1984).

Before synchrotron data acquisition, the anterior and postero-lateral regions were extracted and defatted for 12 h in dichloromethane ($C_2H_2Cl_2$) solution. The specimens were finally dried by exposure to air at room temperature for 48 h.

Ethical approval for collection of samples was granted by the Human Ethics Committee of the Institute of Anatomy at the University René Descartes (Paris, France). The tissue donors or their legal guardians provided informed written consent to provide their tissues for investigation, in accord with legal clauses stated in the French Code of Public Health (Code de la Santé Publique Français).

2.2. Acoustic microscope SAM200Ex

A custom scanning acoustic microscope was used. It consists of a three-axis high-precision scanning stage, a 200 MHz pulser/receiver (Panametrics 5900PR, Waltham, USA) and a 500 MS s^{-1} A/D-card (Gage CS8500, Gage Applied Technologies, Inc., Lachine, Canada). All components are controlled by a custom software (SAMEx, Q-BAM, Halle, Germany). A spherically focused transducer (KSI200/60°: KSI, Herborn, Germany) provided a spatial resolution of approximately 8 μ m. The confocal pulse-echo and frequency spectrum are illustrated in figure 1.

The samples were completely immersed in a temperature-controlled tank filled with distilled, degassed water at 25 °C. The sample surfaces were placed in the focal plane of the transducer and the transducer was scanned in a rectangular plane parallel to the sample surface (C-scan), whereas for each scanned point the entire pulse-echo signal was stored. A scan increment of 4 μ m was chosen for the acquisition.

2.3. Impedance calibration and evaluation

Homogeneous reference materials were used for the impedance calibration and defocus correction, as described elsewhere (Raum *et al* 2004). Since the sampling frequency of the microscope is close to the Nyquist limit for the used acoustic frequency, the reflection amplitude was determined from the power spectrum $S(f)$ of the time-gated signal (figure 1). For gating, a Hamming window with a width of twice the pulse duration, centred around the

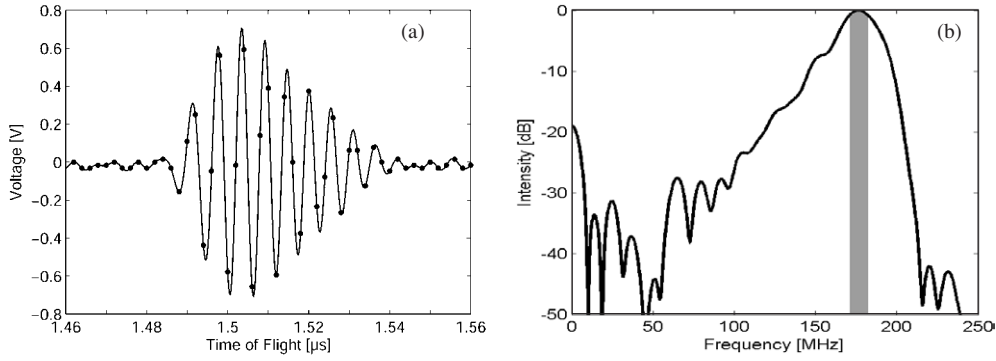


Figure 1. Confocal pulse-echo (a) and power spectrum (b) of the KSI200/60° transducer. The time signal has been interpolated for better illustration. The dots indicate the sampled points. The spectral integration range (175–185 MHz) used for calculating the integrated spectral intensity (ISI) is marked in grey.

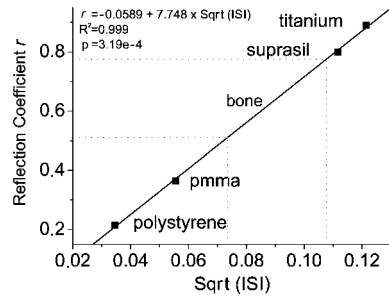


Figure 2. Impedance calibration. For four reference materials the square root of the confocal integrated spectral intensity was correlated with the known reflection coefficients. The range of values measured in the bone tissue is marked with dotted lines.

peak of the Hilbert-transformed echo signal, was applied. The integrated spectral intensity ISI is

$$ISI = \int_{f_1}^{f_2} S(f) df, \quad (1)$$

where $f_1 = 175$ MHz and $f_2 = 185$ MHz are the integration limits. The square root of the ISI values were correlated with the known reflection coefficients of reference materials (figure 2).

Time of flight TOF was determined from the slope of the unwrapped phase spectrum within the bandwidth of the transducer:

$$TOF = t_0 + t_{ph} = t_0 + \frac{\partial \phi}{\partial \omega} = t_0 + \frac{\partial N}{\partial f}, \quad (2)$$

where ϕ is the phase, $\omega = 2\pi f$ is the angular spectrum and t_{ph} is the time relative to the start time of the sequence and N is the number of phase rotations (Kim and Grill 1998).

For the C-scan data the calculated ISI values were defocus corrected using a TOF-dependent correction function (Raum *et al* 2004), converted into reflection coefficients r and finally into values of the acoustic impedance (Z , 1 rayl = 1 kg m⁻² s⁻¹) using the relation

$$r = \frac{Z_2 - Z_1}{Z_2 + Z_1}, \quad (3)$$

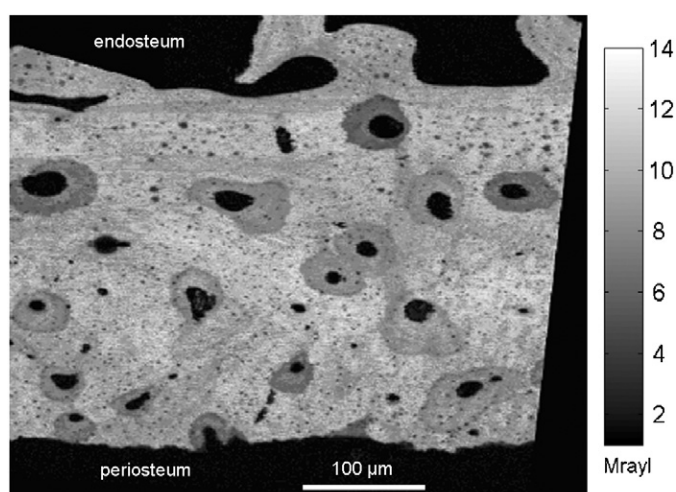


Figure 3. Calibrated acoustic impedance image. Secondary osteons, interstitial tissue and osteocyte lacunae (small dark spots) can be distinguished.

where Z_1 and Z_2 are the impedances in the coupling fluid and in the sample, respectively. Figure 3 shows an example of a calibrated impedance image.

2.4. Synchrotron acquisition

After SAM inspection, the samples were imaged using synchrotron radiation microtomography (SR- μ CT) at the ESRF (European Synchrotron Radiation Facility, Grenoble, France). The experiments were performed on beamline ID19, where a 3D parallel beam μ CT set-up has been developed (Salome *et al* 1999). The system is operational for acquiring three-dimensional images of bone samples at various spatial resolutions (voxel sizes between 15 μ m and 0.3 μ m). Since the aim of the experiment was to compare the SAM and SR- μ CT images, we selected a pixel size on the detector of 4.9 μ m corresponding to a spatial resolution of 10 μ m. Using the 2048 \times 2048 CCD-based 2D detector, this choice enables to get a field of view of 10 \times 10 mm² and thus to encompass the entire cortical sample. Different insertion devices (one wiggler and two undulators) conditioning the spectrum and spreading of the beam may be used on the beamline. Undulators produce higher intensity and more focused ray-like spectrum. Due to the sample size ($\sim 7 \times 5 \times 4$ mm³), it was possible to use the U32 undulator. The energy was set to 23.3 keV (obtained as the third harmonic of the U32 undulator with a gap of 19 mm). As compared to the wiggler, the intensity of the beam was increased by a factor of 10 and the acquisition time was limited to 2 s by view. For each sample, 900 radiographic images under different angles of view were recorded.

The 3D images were then obtained by applying an exact tomographic reconstruction algorithm, based on filtered backprojection (figure 4). The size of the cubic voxel in the reconstructed images was 4.9 μ m. A 3D volume of interest (VOI) made of 1300 \times 900 \times 600 voxels was reconstructed in each sample. The mean degree of mineralization of bone (DMB, g cm⁻³) was derived from the measurement of the local grey levels of the voxels of the segmented 3D volume. Grey levels were converted to volumetric tissue mineralization expressed as g cm⁻³ of hydroxyapatite crystals, as detailed in Nuzzo *et al* (2002).

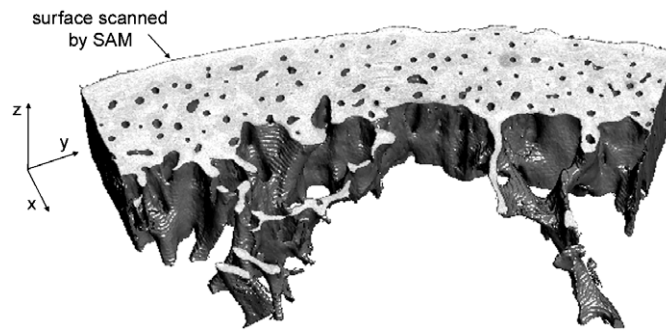


Figure 4. 3D volume reconstruction of a postero-lateral section imaged by SR- μ CT. Each volume data set was sequentially rotated around the x and y axes until the upper cross section surface, which has been scanned by SAM before, was parallel to the xy -plane.

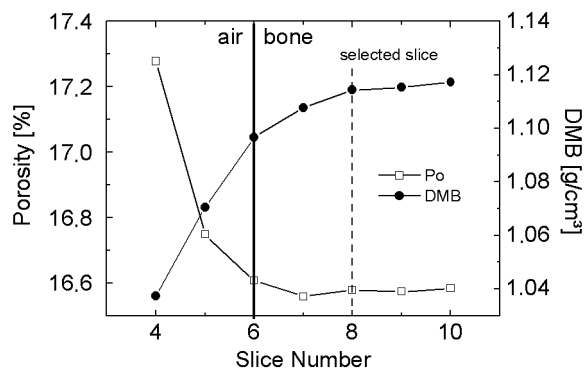


Figure 5. Slice selection for the SR- μ CT surface cross-section reconstruction. Due to the partial volume effect the slice at the surface boundary (air/bone) exhibits decreased mean DMB and increased Po values. The first slice, for which the parameters reached a steady state (vertical dashed line), was used for further analysis. In the example, the selected slice corresponds to a layer approximately $9 \mu\text{m}$ below the surface.

2.5. Image reconstruction and parameter extraction

Several steps were necessary to ensure site-matched analysis of the SAM and SR- μ CT images. Each 3D reconstructed SR- μ CT volume was sequentially rotated around the x and y axes in order to ensure that the cross-section surface scanned with the acoustic microscope is parallel to the xy -plane (figure 4). Then, mean DMB and porosity were calculated for subsequent z -slices above and below the bone boundary. It can be seen in figure 5 that due to the partial volume effect both parameters gradually increase or decrease at the boundary. The first slice beyond the boundary, for which a steady state was reached, was used for further analysis. Then, tissue was segmented from the Haversian canals using threshold masks (Raum *et al* 2003, 2004). Thresholds were set to the mean of tissue and noise level (DMB = 0.6 g cm^{-3} ; $Z = 4 \text{ Mrayl}$). From these binary images, the structural parameters N.Ca (number of detected canals N.Ca), porosity Po (ratio between the area covered by the Haversian canals and total selected bone area, %) and median canal diameter Ca.Dm (the equivalent diameter was determined from the area of the individual canals, μm) were extracted.

For mineral density and impedance estimation, the binary masks were eroded using a disc with a radius of one pixel. This procedure ensured exclusion of boundary pixels for which

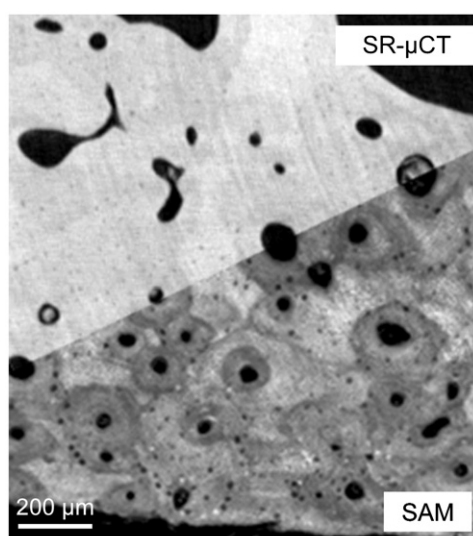


Figure 6. Detail of a fused acoustic impedance Z (SAM) and DMB (SR- μ CT) image. For a better illustration the diagonal line separates regions, for which either the SAM or the SR- μ CT image is in the foreground.

DMB or Z values might have been artificially reduced due to the partial volume effect. The SAM images were then spatially fused with the synchrotron images using the image registration tools of Matlab 6.5 (The Mathworks Inc., Natick, MA, USA). After rigid transformation of the SAM image (rotation, rescaling and translation) final adjustment was achieved by translating the SAM image, until the two-dimensional cross correlation between the two images was maximized. An example of fused SR- μ CT and SAM images is shown in figure 6. This image preprocessing allowed direct comparison of DMB and Z on identical regions of interest (ROI).

2.6. Data analysis

Linear regression analysis, Student's t -test and Bland–Altman plots (Bland and Altman 1986) were used to compare structural parameters derived from the SR- μ CT and SAM measurements. Individual, regional and age influences on the derived tissue properties were investigated with ANOVA. Regression analysis and Pearson correlation coefficients were used to describe the relation between DMB and Z . All statistical results were considered significant for p -values less than 0.05. The statistical computations were made using the Matlab Statistics Toolbox (The Mathworks Inc., Natick, MA, USA).

3. Results

3.1. Accuracy and reproducibility

SAM: six bone samples were measured two times at different days. The average relative reproducibility error of the estimated mean impedances given by the root-mean-square average of the six relative standard deviations was 0.95%. **SR- μ CT:** the relative error of DMB estimation was previously determined to be 0.26% (Nuzzo *et al* 2002).

Table 1. Mean, standard deviation and range of acoustic impedance and mineral density for all investigated ROIs. *Z* and DMB were significantly higher in the interstitial tissue compared to the osteonal tissue (unpaired *t*-test, $p < 10^{-4}$).

	Interstitial	Osteon
<i>N</i>	190	180
<i>Z</i> (Mrayl)	9.3 ± 1.0 (6.6–12.1)	7.2 ± 1.1 (5.1–11.0)
DMB (g cm ⁻³)	1.16 ± 0.05 (1.05–1.28)	1.06 ± 0.07 (0.77–1.21)

3.2. Morphology

Structural parameter estimations of N.Ca, Ca.Dm and Po obtained from the SR- μ CT and SAM images were compared for the entire overlapping image areas ($N = 18$). Endosteal regions with apparent huge pores were excluded from the analysis. The Pearson correlation coefficients of the linear regression between SAM and SR- μ CT parameter estimations were highly significant ($R^2 > 0.72$, $p < 0.0001$). The best correlation was found for the estimation of the number of Haversian canals within the evaluated ROIs ($N.Ca_{SAM} = 1.35 + N.Ca_{SR-\mu CT}$, $R^2 = 0.97$, RMSE = 5.6). There was a general trend for an overestimation of the structural parameters with SAM compared to SR- μ CT (figure 7). The Haversian canal densities (number of Havers canals per unit area N.Ca/Ar) derived from the SR- μ CT and SAM images were $10.4 \pm 4.8 \text{ mm}^{-2}$ and $10.8 \pm 5.3 \text{ mm}^{-2}$, respectively. The average relative difference was $-2.1 \pm 2.4\%$ (mean and standard error), but this difference was not significant (paired *t*-test, $p = 0.22$). The medians of Ca.Dm determined within the 18 evaluated regions were in the range between 36 and 74 μm ($Ca.Dm_{SR-\mu CT} = 54.3 \pm 9.3 \mu\text{m}$, $Ca.Dm_{SAM} = 54.9 \pm 9.5 \mu\text{m}$). The average relative difference of $-0.8 \pm 2.6\%$ (figure 7(b)) was not significant (paired *t*-test, $p = 0.68$).

Figure 7(c) shows that the average porosity estimation was 0.8% lower in the SR- μ CT images than in the SAM images. The mean and standard deviations were $Po_{SR-\mu CT} = 5.7 \pm 2.4\%$ and $Po_{SAM} = 6.5 \pm 2.3\%$. The relative bias of $-13.1 \pm 3.8\%$ was significantly different from zero (paired *t*-test, $p < 0.05$).

3.3. Tissue properties

DMB and *Z* were evaluated in site-matched ROIs within the fused images. Small ROIs were chosen manually either in osteonal or interstitial tissue. The selected ROIs were large enough to contain a statistically relevant number of sample points (e.g., 500–1000 points for a single osteon after removal of area occupied by the Haversian canal and osteocyte lacunae). From each of the ten bone samples approximately 20–30 osteons and regions of interstitial tissue were selected. DMB and impedance values were in the range between 0.77 and 1.28 g cm⁻³ and 5.13 and 12.1 Mrayl, respectively. The interstitial tissue DMB was approximately 23% higher and the impedance was 29% higher compared to the values obtained in osteonal tissue (table 1). The differences were statistically significant (paired *t*-test, $p < 0.05$).

Figure 8 shows the relation between DMB and *Z*. A weak, but significant correlation was obtained for the osteonal ($R^2 = 0.174$, $p < 10^{-4}$) but not for the interstitial tissue data. The pooled (osteonal and interstitial) data follow a second-order polynomial ($R^2 = 0.39$, $p < 10^{-4}$).

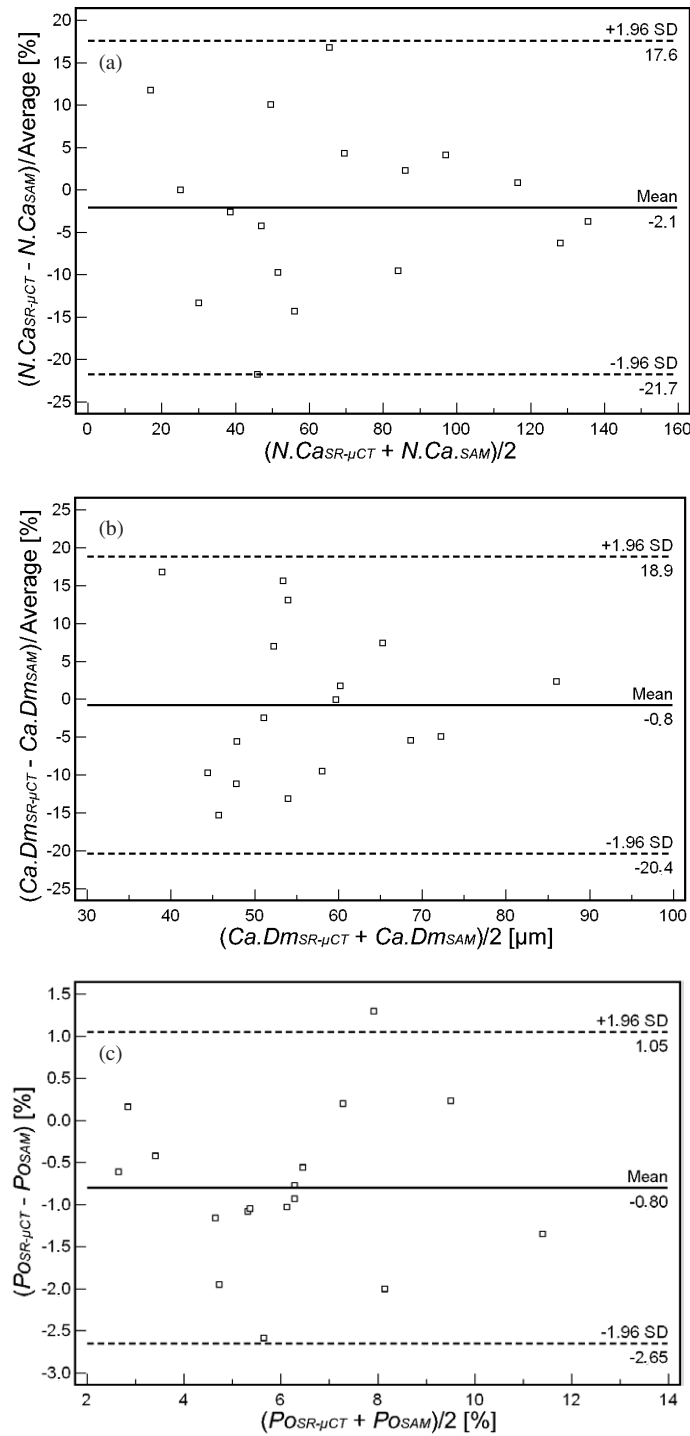


Figure 7. Bland–Altman plots show the comparison of N.Ca, Ca.Dm and Po estimations from the SR- μ CT and SAM images (the first two parameters are displayed as percentage differences).

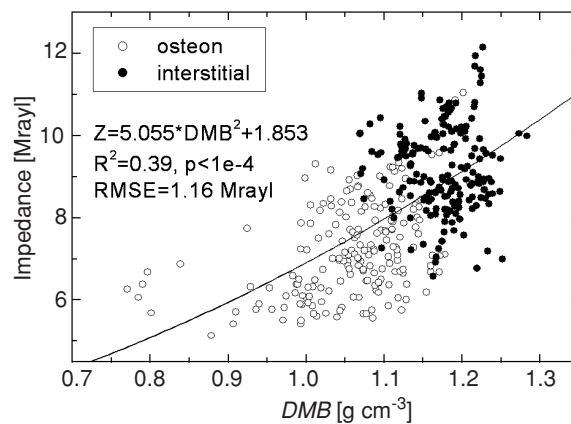


Figure 8. Relation between degree of mineralization and acoustic impedance for osteonal and interstitial tissues. The values were obtained from site-matched ROIs ($N_{\text{osteon}} = 190$, $N_{\text{interstitial}} = 180$), for which Haversian canals and osteocyte lacunae were excluded.

Table 2. One-way ANOVA for DMB and Z (F -statistic and p -values). Categorical factors are: sample index (1, ..., 10), region (anterior/postero-lateral), tissue type (osteonal/interstitial), age and gender. Except for the gender all factors had significant influences on the variances of both tissue parameters.

Factor	DMB		Z	
	F	p	F	p
Sample index	8.11	<0.0001	11.54	<0.0001
Region	9.92	<0.0001	6.06	0.0142
Tissue	362.89	<0.0001	540.23	<0.0001
Age	9.13	<0.0001	8.33	<0.0001
Gender	3.69	0.0552	2.50	0.1141

3.4. Interindividual variations of tissue properties

One-way ANOVA of DMB and Z with sample index, anatomical region (anterior and postero-lateral), tissue type (osteonal and interstitial), age or gender as categorical factors showed that except for the gender all factors contribute significantly to the variances of DMB and Z (table 2). The F -values obtained for the tissue type were much higher than those of the other factors. Three-way ANOVA with age, anatomical region and tissue type confirms the strong impact of the tissue type and the moderate, but significant influences of age and anatomical region on both tissue properties (table 3). Moreover, the second-order interaction terms between age and tissue type suggest that the difference between osteonal and interstitial tissue parameters is also age dependent. The other interactions terms were not significant. The age distribution of the sample population was not normal (Lilliefors test, $p > 0.05$). Therefore, the data were divided into two normally distributed age groups (with ages below and above 75 years) for further evaluation of the age dependence (table 4). ANOVA followed by post hoc Tukey test for multiple comparison of means revealed increased DMB values in interstitial tissue compared to osteonal tissue, but no age dependences within the two tissue types ($F = 121$, $p < 0.0001$). The impedance values were significantly different in each group,

Table 3. Three-way ANOVA for DMB and Z (df: degrees of freedom, SS: sums of squares, F : F -statistic, p : p -value). The analysis was restricted to two-factor interaction terms and only significant interaction terms are shown. The values were computed using the constrained sums of squares (SS). Categorical factors are: age, region (anterior/postero-lateral) and tissue type (osteonal/interstitial).

Factor	DMB				Z		
	df	SS	F	p	SS	F	p
Age	8	0.419	20.9	<0.0001	145.9	24.3	<0.0001
Region	1	0.036	14.4	0.0002	9.6	12.8	0.0004
Tissue	1	1.359	541.3	<0.0001	513.7	683.7	<0.0001
Age*tissue	8	0.111	5.6	<0.0001	23.2	3.9	0.0002

Table 4. Mean and standard deviation of DMB and Z for osteonal (os) and interstitial (is) tissues for different age groups. While Z was significantly different in each group, differences of DMB were only found between the two tissue types (ANOVA followed by multiple comparison Tukey test).

Age	Tissue	N	DMB (g cm^{-3})	Z (Mrayl)
<75	os	150	1.06 ± 0.08	7.41 ± 1.13
	is	158	1.16 ± 0.04	9.53 ± 0.99
>75	os	78	1.06 ± 0.06	6.77 ± 0.78
	is	99	1.17 ± 0.05	8.95 ± 1.01

e.g., interstitial tissues had higher values than osteonal tissue and each tissue type had lower values in the older age group compared to the younger age group ($F = 189$, $p < 0.0001$).

4. Discussion

High-resolution imaging modalities give access to material properties at the tissue level independently of microstructure. In a previous study, Raum *et al* (2004) investigated the frequency and resolution dependences of structural parameter estimations from SAM images in the frequency range from 25 to 100 MHz. They concluded that a resolution of at least $20 \mu\text{m}$ would be required for a reliable parameter estimation in compact bone. The spatial resolution of both techniques used in this study was at least $10 \mu\text{m}$ and confirmed to be sufficient to separate the Haversian canals from the tissue. Therefore, structural parameter estimations obtained from radiographic and acoustic images were almost identical. Although not directly comparable the estimated values are in the range of histomorphometric values measured in human femoral bone. For example, Stein *et al* (1999) evaluated over 400.000 pores in a population of 96 specimens from human subjects aged 21–92 years. The reported cohort medians (and interquartile ranges) of porosity, number of pores and pore area were 5.9% (4.3–7.9%), 10.1 mm^{-2} (8.8 – 12.2 mm^{-2}) and $2050 \mu\text{m}^2$ (1700 – $2500 \mu\text{m}^2$), respectively. With the assumption of a circular cross section the corresponding median (and interquartile range) of the pore diameter is $51 \mu\text{m}$ (46 – $56 \mu\text{m}$). Osteocyte lacunae could only be distinguished from the tissue in the acoustic images. In the SR- μ CT images, the lacunae were identified as small spots with slightly reduced grey-level values compared to the surrounding tissue (see figure 6). The decrease, however, was not large enough to use a threshold for the segmentation. The

osteocytes have an average diameter of approximately $4\ \mu\text{m}$ (Wang and Ni 2003). Under the assumption of a spherical shape the volume of one lacuna would be $33\ \mu\text{m}^3$ and one image voxel of $(4.9\ \mu\text{m})^3 = 118\ \mu\text{m}^3$ would still contain approximately 72% of mineralized tissue, if the osteocyte would be located completely within the voxel. In the worst case, it could be located in the centre of four voxels, and each voxel would contain approximately 7% of the osteocyte lacuna. Thus, it can be concluded that due to the partial volume effect the estimated DMB in voxels containing an osteocyte is in the order of 70–93% of the surrounding tissue DMB. On the other hand, the osteocyte density in cortical bone is typically in the range between $400\ \text{mm}^{-2}$ and less than $1000\ \text{mm}^{-2}$ (Hernandez *et al* 2004, Vashishth *et al* 2002), which corresponds to 0.024 lacunae per voxel or less in the SR- μCT data. Therefore, the underestimation of tissue DMB in the evaluated regions of interest due to the osteocyte lacunae is approximately in the range between 0.3 and 0.7%.

Acoustic impedance Z and degree of mineralization DMB provide complementary information about the tissue properties. It has been demonstrated that Z reflects elastic anisotropy and correlates well with Young's modulus obtained by nanoindentation (Hofmann *et al* 2006, Raum *et al* 2004). The global shape of the correlation between Z and DMB follows a second-order polynomial and the extrapolated impedance for completely demineralized bone tissue ($Z = 1.85\ \text{Mrayl}$) corresponds well with literature values for nonmineralized dense collagen. For example, Toyras *et al* (2002) and Leicht *et al* (2004) reported values for articular cartilage in the range between 1.6 and 2.1 Mrayl. However, the poor correlation coefficient and large root-mean-square error ($\text{RMSE} = 1.16\ \text{Mrayl}$) suggest additional factors that are not accounted for in this regression model. For example, it is well accepted that bone tissue is anisotropic and it has been reported that the degree of elastic anisotropy varies between osteonal and interstitial tissues (Rho *et al* 2001). Since DMB is not sensitive to elastic anisotropy it is likely that the relation between DMB and Z depends on the probing direction. Other factors, e.g. collagen cross linking, size and interconnection of mineral platelets, will affect the elastic properties but will not affect the mineral density measurement. However, in order to elucidate the impact of structure and composition on the tissue elasticity, the principal relations between tissue degree of mineralization, mass density, acoustic impedance and elastic coefficients need to be resolved. This is the objective of a companion paper (Raum *et al* 2006).

Although a comprehensive investigation of the age dependences of DMB and Z was beyond the scope of this study, our data confirm a previous microradiography investigation, in which no age-related change of the degree of mineralization in a broad population of 43 human subjects was observed (Boivin and Meunier 2002). The mean degree of mineralization of $1.082 \pm 0.017\ \text{g cm}^{-3}$ was comparable to the values we observed in our study. However, we found a significant decrease of acoustic impedance with age in osteonal and interstitial tissues that was not associated with a loss of mineralization. As discussed above, the reasons for this can be multifold and merit further investigation. Nonetheless our findings suggest that SAM provides complementary information on the elastic tissue state that is not depicted by the measurement of mineral density.

5. Conclusions

High-resolution SR- μCT and 200 MHz SAM fulfil the requirement for a simultaneous evaluation of cortical bone microstructure and material properties at the tissue level. While SAM inspection is limited to the evaluation of carefully prepared sample surfaces, SR- μCT provides volumetric information on the tissue without substantial preparation requirements. However, the main advantage of SAM is to provide a quantitative estimate of elastic properties at the tissue level that cannot be captured by SR- μCT . The capability of mapping

microstructure, mineralization and elastic properties of bone tissue with a scalable resolution from the organ level down to the cellular level is of great interest for a variety of bone research fields:

- (1) Ageing or osteoporosis affects the elastic and ultimate properties of bone as shown by mechanical testing, but little is known about the effect of elastic changes at a microscale on macroscopic properties. Micro-scanning the elastic properties offers a unique promise to gain insight into the relation between microscopic and macroscopic mechanical alterations.
- (2) The demand for high-resolution micro-elastic screening techniques is rapidly increasing with the progress in molecular biology. A number of different genes have been targeted to play a role in the regulation of skeletal metabolism and small animals with specific genetic modifications have become the model of choice for studying the genetic or therapeutic effects on the elastic bone phenotype and its microstructure. Quantitative SR- μ CT and SAM are two candidates with sufficient resolution and rapid screening capabilities to assess the spatial distribution of relevant tissue properties in three or two dimensions, respectively.
- (3) Because sound propagation velocity measured with an axial transmission ultrasound device in the human radius can be predicted by microstructural and tissue material parameters such as elasticity and mineralization (Raum *et al* 2005), a better knowledge of bone properties at a microscale may lead to an optimization of non-invasive ultrasound devices for the assessment of bone fragility, e.g., to separately measure changes in microstructure, mineralization and/or elasticity following disease progression or response to therapy.
- (4) The heterogeneity of tissue properties we report here substantiates the importance of 'real-life' elastic input data for numerical simulations such as finite-element analysis.

Acknowledgments

The authors are grateful for the financial support by the DAAD PPP Program no D/0122910, the Deutsche Forschungsgemeinschaft, Grant Ra 1380/1-1 and the MAE Program PAI PROCOPE 04544UM. One author (K Raum) acknowledges support from CNRS (Poste Chercheur Associé).

References

- Bland J M and Altman D G 1986 Statistical methods for assessing agreement between two methods of clinical measurement *Lancet* **1** 307–10
- Boivin G and Meunier P J 2002 The degree of mineralization of bone tissue measured by computerized quantitative contact microradiography *Calcif. Tissue Int.* **70** 503–11
- Bousson V, Peyrin F, Bergot C, Hausard M, Sautet A and Laredo J D 2004 Cortical bone in the human femoral neck: three-dimensional appearance and porosity using synchrotron radiation *J. Bone Miner. Res.* **19** 794–801
- Hengsberger S, Enstroem J, Peyrin F and Zysset P 2003 How is the indentation modulus of bone tissue related to its macroscopic elastic response? A validation study *J. Biomech.* **36** 1503–9
- Hernandez C J, Majeska R J and Schaffler M B 2004 Osteocyte density in woven bone *Bone* **35** 1095–9
- Hofmann T, Heyroth F, Meinhard H, Fraenzel W and Raum K 2006 Assessment of composition and anisotropic elastic properties of secondary osteon lamellae *J. Biomech.* at press
- Kim T J and Grill W 1998 Determination of the velocity of ultrasound by short pulse switched sinusoidal excitation and phase-sensitive detection by a computer-controlled pulse-echo system *Ultrasonics* **36** 233–8
- Leicht S, Raum K and Brandt J 2004 Quantitative SAM investigation of changes in cartilage and subchondral bone due to primary arthritis *Technol. Health Care* **12** 174–6

- Linde F and Sorensen H C 1993 The effect of different storage methods on the mechanical properties of trabecular bone *J. Biomech.* **26** 1249–52
- Nuzzo S, Peyrin F, Cloetens P, Baruchel J and Boivin G 2002 Quantification of the degree of mineralization of bone in three dimensions using synchrotron radiation microtomography *Med. Phys.* **29** 2672–81
- Pelker R R, Friedlaender G E, Markham T C, Panjabi M M and Moen C J 1984 Effects of freezing and freeze-drying on the biomechanical properties of rat bone *J. Orthop. Res.* **1** 405–11
- Peyrin F, Muller C, Carillon Y, Nuzzo S, Bonnassie A and Briguet A 2001 Synchrotron radiation microCT: a reference tool for the characterization of bone samples *Adv. Exp. Med. Biol.* **496** 129–42
- Pothuaud L, Laib A, Levitz P, Benhamou C L and Majumdar S 2002 Three-dimensional-line skeleton graph analysis of high-resolution magnetic resonance images: a validation study from 34-micron-resolution microcomputed tomography *J. Bone Miner. Res.* **17** 1883–95
- Raum K, Cleveland R O, Peyrin F and Laugier P 2006 Derivation of elastic stiffness from site-matched mineral density and acoustic impedance maps *Phys. Med. Biol.* **51** 747–58
- Raum K, Jenderka K V, Klemenz A and Brandt J 2003 Multi layer analysis—quantitative scanning acoustic microscopy for tissue characterization at a microscopic scale *IEEE Trans. Ultrason. Ferroelectr. Freq. Control* **50** 507–16
- Raum K, Leguerey I, Chandelier F, Bossy E, Talmant M, Saïed M, Peyrin F and Laugier P 2005 Bone microstructure and elastic tissue properties are reflected in QUS axial transmission measurements *Ultrasound Med. Biol.* **31** 1225–35
- Raum K, Reisschauer J and Brandt J 2004 Frequency and resolution dependence of the anisotropic impedance estimation in cortical bone using time-resolved scanning acoustic microscopy *J. Biomed. Mater. Res. A* **71** 430–8
- Rho J Y, Currey J D, Zioupos P and Pharr G M 2001 The anisotropic Young's modulus of equine secondary osteones and interstitial bone determined by nanoindentation *J. Exp. Biol.* **204** 1775–81
- Salome M, Peyrin F, Cloetens P, Odet C, Laval-Jeantet A M, Baruchel J and Spanne P 1999 A synchrotron radiation microtomography system for the analysis of trabecular bone samples *Med. Phys.* **26** 2194–204
- Stein M S, Feik S A, Thomas C D, Clement J G and Wark J D 1999 An automated analysis of intracortical porosity in human femoral bone across age *J. Bone Miner. Res.* **14** 624–32
- Toyras J, Nieminen H J, Laasanen M S, Nieminen M T, Korhonen R K, Rieppo J, Hirvonen J, Helminen H J and Jurvelin J S 2002 Ultrasonic characterization of articular cartilage *Biorheology* **39** 161–9
- Vashishth D, Gibson G, Kimura J, Schaffler M B and Fyhrie D P 2002 Determination of bone volume by osteocyte population *Anat. Rec.* **267** 292–5
- Wachter N J, Augat P, Krischak G D, Mentzel M, Kinzl L and Claes L 2001 Prediction of cortical bone porosity *in vitro* by microcomputed tomography *Calcif. Tissue Int.* **68** 38–42
- Wachter N J, Krischak G D, Mentzel M, Sarkar M R, Ebinger T, Kinzl L, Claes L and Augat P 2002 Correlation of bone mineral density with strength and microstructural parameters of cortical bone *in vitro* *Bone* **31** 90–5
- Wang X and Ni Q 2003 Determination of cortical bone porosity and pore size distribution using a low field pulsed NMR approach *J. Orthop. Res.* **21** 312–9
- Xu J, Rho J Y, Mishra S R and Fan Z 2003 Atomic force microscopy and nanoindentation characterization of human lamellar bone prepared by microtome sectioning and mechanical polishing technique *J. Biomed. Mater. Res. A* **67** 719–26
- Zysset P K, Guo X E, Hoffer C E, Moore K E and Goldstein S A 1999 Elastic modulus and hardness of cortical and trabecular bone lamellae measured by nanoindentation in the human femur *J. Biomech.* **32** 1005–12